Kamel Hooman (2009) Applied thermal Engineering (29) 1012-1019

Slip flow forced convection in a microporous duct of rectangular cross-section

K. Hooman

School of Engineering, The University of Queensland, Brisbane, Australia

Abstract

Applying a Fourier series approach, closed form solutions for fully developed velocity and temperature distribution in a porous-saturated microduct of rectangular cross-section are presented in the slip-flow regime. The Brinkman flow model is applied. Invoking the temperature jump equation, the **H1** thermal boundary condition is investigated. Expressions are presented for the local and average velocity and temperature profiles, the friction factor, and the slip coefficient in terms of the key parameters. The present results, which are applicable to microducts of rectangular cross-section filled with or without a porous medium, are found to be in complete agreement with those available in the literature for both no-slip and slip flow regime.

Keywords; MEMS, Fourier series approach, Microporous, Slip flow, Temperature jump

Nomenclature

a	channel width to height ratio
A	cross-sectional area [m^2]
B	coefficient
C	microduct inside periphery [m]
c_P	specific heat at constant pressure [$J/kg{\cdot}K$]
Da	Darcy number, K/H^2
D_H	hydraulic diameter $4Ha/(a+1)$ [m]
D_n	coefficient
f	friction factor

F	tangential momentum accommodation coefficient
F_t	thermal accommodation coefficient
g,g^+	auxiliary functions
h	heat transfer coefficient [$W/m^2.K$]
H	half microduct width [m]
k	porous medium thermal conductivity [$W/m{\cdot}K$]
K	permeability [m^2]
Kn	Knudsen number, $Kn= \lambda/D_H$
L	Microchannel length [m]
m	parameter $(s^2+\lambda_n^2)^{1/2}$
M	viscosity ratio, μ_{eff}/μ
n	(coordinate) normal to the wall, [m]
Nu	Nusselt number
P^*	pressure, [Pa]
Pr	Prandtl number
q''	wall heat flux [W/m^2]
R	thermal resistance [mK/W]
Re	Reynolds number, $Re= \rho U^* D_H/\mu$
s	porous media shape parameter, $s=(MDa)^{-1/2}$
T^*	local temperature [K]
u^*	x-velocity [m/s]
$\hat{u}$	normalized velocity
U^*	average velocity [m/s]
v	auxiliary function

x^* longitudinal coordinate [m]

y^*,z^* transverse coordinates [m]

y,z $(y^*,z^*)/H$

Greek symbols

β slip coefficient

ε porosity

η coefficient, $\eta = \beta B$

Γ tangential coordinate at the microduct wall inside periphery, m

γ specific heat ratio

λ molecular mean free path [m]

λ_n eigenvalue, $\lambda_n=(2n-1)\pi/2$

θ dimensionless temperature

μ fluid viscosity [$N \cdot s/m^2$]

μ_{eff} effective viscosity [$N \cdot s/m^2$]

ρ fluid density [kg/m^3]

Superscripts

$*$ dimensional

Subscripts

f fluid

in inlet

m mean

o outlet

pm porous matrix

s slip

w wall

1. Introduction

Analysis of heat and fluid flow at microscale is of great importance not only for the need for high heat flux in small electronic devices but also for playing a key role in the biological systems. Modeling heat and fluid flow through such small devices, with their size being in the order of a few 100 microns, is different from the macroscale counterparts in being associated with the inclusion of velocity slip, temperature jump, and other newly developed issues (Ameel et al. 1997). For example, a gaseous flow at such small passage does not obey the classical continuum physics where the no-slip condition is valid. Consequently, such a flow is associated with a nonzero fluid velocity at the solid walls and there exists a difference between the gas temperature and that of the wall. According to Ghoddoosi and Egrican (Ghodoossi and Egrican 2005), who studied microchannel heat transfer under slip flow and **H1** boundary condition, this can happen when $0.001<Kn<0.1$ while the flow is called slip flow. On the other hand, it is known that for the above range of *Kn* results obtained based on continuum assumptions match experimental counterpart provided that corrections in terms of the slip velocity and temperature jump be applied (Renksizbulut, Niazmand and Tercan 2006).

Slip flow in various-shaped microchannels has been studied extensively in the past decades (Morini, Spiga and Tartarini 2004, Sparrow and Hajisheikh 1964, Zhu and Liao 2006, Tunc and Bayazitoglu 2002, Zhu, Liao and Xin 2006, Yu and Ameel 2001, Hooman 2007), to name a few. However, theoretical research on slip flow in porous-saturated microducts of arbitrary cross-section has not been conducted as much as those on clear fluid counterparts. The problem becomes more complicated when one notes that only a handful of papers, see for example (Hooman, Haji-Sheikh and Nield 2007, Hooman and Merrikh 2006, Haji-Sheikh, Nield and Hooman 2006, Haji-Sheikh, Minkowycz and Sparrow 2004, Haji-Sheikh 2006, Hooman and Gurgenci 2007a, Hooman, Gurgenci and Merrikh 2007, Haji-Sheikh and Vafai 2004, Merrikh and Lage 2005), can be mentioned when it comes to name analytical studies on macro-porous ducts of cross-sections other than circular tube or Parallel Plate Channel (PPC), say rectangular shape,

even when the saturating fluid is not a rarefied gas. Analytical solutions are not only very useful in benchmarking numerical computations but also they are very powerful for parametric studies when a large number of parameters are involved wherever numerical results cannot be experimentally verified, or no experiments are possible due to time, cost, and other limiting factors. Thus, the question naturally arises as to whether analytical solutions for ducts of cross-section other than circular tube or parallel plates are possible when the fluid saturating the porous microchannel is a rarefied gas. Some of the slip flow studies in microporous ducts are summarized here. Haddad et al. (Haddad, Ali-Nimr and Taamneh 2006) have numerically studied slip flow forced convection in micro-PPC to observe that the skin friction is increased by increasing the Darcy number, decreasing the Knudsen number, and the Forchheimer number. Moreover, they reported that heat transfer increases as the modified Reynolds number and Darcy number increase while it decreases as the Knudsen/Forchheimer number increases. In a subsequent study, Haddad et al. (Haddad, Al-Nimr and Abuzaid 2006) analyzed the effect of frequency of fluctuation of the driving force on basic slip flows in the presence of a porous medium for transient Couette flow, the pulsating Poiseuille flow, the Stokes second problem, and the transient natural convection flow. Available in their report is the fact that the increase in frequency or the Knudsen number would lead to increase in the normalized slip for all of the four aforementioned problems. On the other hand, the normalized slip was found to increase as the Darcy number plunges, except for Poiseuille flow where the normalized slip increased as it was increased. According to their findings, the temperature-jump is negligible when the frequency and the Knudsen number are small. Local thermal non-equilibrium effects on slip flow forced convection in a micro-porous PPC was also studied by (Haddad, Al-Nimr and Al-Omary 2007). Nield and Kuznetsov (Nield and Kuznetsov 2006) dealt with slip flow in microtubes or micro-PPC saturated by a hyperporous medium.

This paper aims at finding the velocity and temperature distribution in a microporous duct of rectangular cross-section under slip flow and **H1** boundary condition. The Fourier series approach (Kreyszig 2006) is applied to solve the momentum and energy equations.

2. Analysis

Consider fully developed forced convection in a microporous duct of rectangular cross-section as shown by Fig. 1. The slip velocity can be found as

$$u_s^* = \frac{F-2}{F} KnD_H \left.\frac{\partial u^*}{\partial n}\right|_{wall} \tag{1}$$

On the other hand, the fluid temperature at the wall, T_s*, can be different from that of the wall, T_w*, i.e.

$$T_s^* - T_w^* = \frac{F_t-2}{F_t} D_H \frac{Kn}{\Pr} \frac{2\gamma}{1+\gamma} \left.\frac{\partial T^*}{\partial n}\right|_{wall} \tag{2}$$

The local values of the slip velocity and the temperature jump change along the duct periphery; however, taking an average over the duct periphery, these averaged values (denoted by an over-bar) would be independent of the coordinates, e.g. with Γ being the tangential coordinate at a point on the microchannel wall inside periphery C, the average values (of slip velocity and temperature jump) are

$$\bar{u}_s^* = \int_C u_s^* d\Gamma / C$$
$$\bar{T}_s^* - \bar{T}_w^* = \frac{F_t-2}{F_t} \frac{2\gamma}{1+\gamma} \frac{Kn}{\Pr} \frac{D_H}{C} \int_C \left.\frac{\partial T^*}{\partial n}\right|_{wall} \tag{3a,b}$$

Moreover, similar to Tunc and Bayazitoglu (Tunc and Bayazitoglu 2002), the slip coefficient, β, is obtainable as

$$\beta = \bar{u}_s^* / U^* \tag{4}$$

where $U^*=\langle u^* \rangle$ is the average velocity with the angle brackets denoting an average taken over the microduct cross-section.

2.1. Hydrodynamic aspects of the problem

The Brinkman momentum equation, to be solved subject to slip condition or Eq. (1), is

$$\mu_{eff}\nabla^2 u^* - \frac{\mu u^*}{K} - \frac{\partial p^*}{\partial x^*} = 0. \tag{5}$$

Scaling the velocity with $-H^2\partial p^*/\partial x^*/\mu$, the following dimensionless velocity

$$v = -\mu(u^* - \bar{u}_s^*)/(H^2\partial p^*/\partial x^*) \tag{6}$$

leads to

$$\nabla^2 v - s^2 v + \frac{1}{M} - s^2\bar{u}_s = 0. \tag{7}$$

that should be solved subject to v=0 at the walls. Hence, the eigenfunction expansion approach (see (Hooman and Merrikh 2006, Hooman and Gurgenci 2007a, Kreyszig 2006, Haji-Sheikh and Vafai 2004)) leads to the following solution for the velocity

$$v = \frac{4}{\pi}\left(\frac{1}{M} - s^2\bar{u}_s\right)\sum_{n=1}^{\infty} D_n\left(1 - \frac{\cosh mz}{\cosh ma}\right)\cos\lambda_n y, \tag{8}$$

where m and D_n are found to be

$$m = (s^2 + \lambda_n^2)^{1/2}$$
$$D_n = \frac{(-1)^{n-1}}{(2n-1)m^2} \tag{9}$$

Based on Eqns. (1) and (3a) the average dimensionless slip-velocity, $\bar{u}_s$, can be found, as

$$\bar{u}_s = \frac{\eta}{Ms^2\eta + 1} \tag{10}$$

with

$$\eta = \frac{2-F}{F} Kn \left(\frac{4a}{1+a} \right)^2 \frac{1}{2M} \sum_{n=1}^{\infty} \frac{1}{m^2} \left(1 + \frac{s^2}{\lambda_n^2} \frac{\tanh ma}{ma} \right) \tag{11}$$

This leads to

$$v = \frac{4}{\pi M} \left(\frac{1}{Ms^2\eta + 1} \right) \sum_{n=1}^{\infty} D_n (1 - \frac{\cosh mz}{\cosh ma}) \cos \lambda_n y \tag{12}$$

The dimensional velocity u^* now takes the following form

$$u^* = -\frac{\partial p^*}{\partial x^*} \frac{H^2}{\mu} \frac{\eta + \frac{4}{\pi M} \sum_{n=1}^{\infty} D_n (1 - \frac{\cosh mz}{\cosh ma}) \cos \lambda_n y}{Ms^2\eta + 1} \tag{13}$$

The mean velocity is thus

$$U^* = -\frac{\partial p^*}{\partial x^*} \frac{H^2}{\mu} \frac{B}{Ms^2\eta + 1}, \tag{14-a}$$

with

$$B = \eta + \frac{2}{M} \sum_{n=1}^{\infty} \frac{1}{m^2 \lambda_n^2} (1 - \frac{\tanh ma}{ma}) \tag{14-b}$$

The normalized velocity is

$$\hat{u} = \frac{\eta + \frac{4}{\pi M} \sum_{n=1}^{\infty} D_n (1 - \frac{\cosh mz}{\cosh ma}) \cos \lambda_n y}{B} \tag{15}$$

The dimensionless pressure drop, represented by *fRe*, reads

$$f \, \mathrm{Re} = \left(\frac{D_H}{2H} \right)^2 \frac{2}{U} = 8 \left(\frac{a}{1+a} \right)^2 \frac{1 + Ms^2\eta}{B} \tag{16}$$

Note that f is the pressure gradient normalized by $2\rho U^{*2}/D_H$. Furthermore, the slip coefficient, β, is now easily obtainable as $\beta = \eta/B$. For $s=0$, that represents a microchannel without a porous insert, one has

$$\eta = \frac{2-F}{F} Kn\left(\frac{a}{1+a}\right)^2 \frac{4}{M}$$

$$f\,\mathrm{Re} = \frac{M}{\frac{2-F}{2F} Kn + \left(\frac{1+a}{2a}\right)^2 \sum_{n=1}^{\infty} \frac{1}{\lambda_n^4}\left(1-\frac{\tanh \lambda_n a}{\lambda_n a}\right)} \qquad \text{(17a-c)}$$

$$\beta = \frac{\frac{2-F}{F} Kn\left(\frac{a}{1+a}\right)^2}{\frac{2-F}{F} Kn\left(\frac{a}{1+a}\right)^2 + \sum_{n=1}^{\infty} \frac{1}{2\lambda_n^4}\left(1-\frac{\tanh \lambda_n a}{\lambda_n a}\right)}$$

Observe for the special case when $M=F=1$ and $a\rightarrow\infty$ that $fRe=24/(1+12Kn)$ which is in line with previous studies (see for example (Renksizbulut et al. 2006) or) and $\beta=12Kn/(1+12Kn)$.

2.1. Thermal aspects of the problem

Assuming local thermal equilibrium, homogeneity, and no thermal dispersion the thermal energy equation reads

$$u^* \frac{\partial T^*}{\partial x^*} = \frac{k}{\rho c_P}\left(\frac{\partial^2 T^*}{\partial y^{*2}} + \frac{\partial^2 T^*}{\partial z^{*2}}\right). \qquad (18)$$

One may consult (Nield and Bejan 2006) to find the condition based on which one can neglect the aforementioned effects in the thermal energy equation. The Nusselt number is defined as

$$Nu = \frac{q'' D_H}{k(T_w^* - T_m^*)}. \qquad (19)$$

with the bulk temperature $T_m^* = \langle \hat{u} T^* \rangle$.

Applying the First Law of Thermodynamics to a thin slice of the microduct, the longitudinal temperature gradient, in terms of the wall heat flux, reads

$$\frac{\partial T^*}{\partial x^*} = \frac{q''}{\rho c_P H U^*} \frac{1+a}{a} \qquad (20)$$

This, in turn, simplifies the thermal energy equation to

$$\hat{u}\frac{q''}{H}\frac{1+a}{a}=k(\frac{\partial^2 T^*}{\partial y^{*2}}+\frac{\partial^2 T^*}{\partial z^{*2}}). \quad (21)$$

Following the definition $\theta=k(T^*-\overline{T}_s^*)/(q''H)$, the dimensionless form of the thermal energy equation will be

$$\nabla^2\theta=\hat{u}\frac{1+a}{a}. \quad (22)$$

that should be solved subject to $\theta=0$ at the walls.

One can assume

$$\theta=\frac{1+a}{as^2}\hat{u}+g(y,z). \quad (23)$$

to have

$$\frac{1+a}{a}\left(\nabla^2\hat{u}-s^2\hat{u}\right)+s^2\nabla^2 g(y,z)=0 \quad (24)$$

One can divide the momentum equation by the average velocity to observe that

$$\nabla^2\hat{u}-s^2\hat{u}=-\frac{1}{MU} \quad (25)$$

which leads to

$$\nabla^2 g(y,z)=\frac{1+a}{aMs^2U} \quad (26)$$

This equation should be solved subject to $g=0$ at the walls; however, it can be even more simplified by assuming

$$g^+(y,z)=\frac{Ms^2Ua}{1+a}g(y,z) \quad (27)$$

to

$$\nabla^2 g^+(y,z)=1 \quad (28)$$

This is very similar to a conduction problem for a rectangular slab with uniform internal heat generation, see Beck et al. (Beck et al. 1992). Therefore, one can use the solutions available in the

open literature. The above methodology is general and is equally applicable to **H1** problems with ducts of other cross-sections.

Alternatively, one can use the Fourier series approach (Kreyszig 2006) to observe that

$$g^{+}(y,z) = 2\sum_{n=1}^{\infty} \frac{(-1)^n}{\lambda_n^3}\left(1 - \frac{\cosh \lambda_n z}{\cosh \lambda_n a}\right)\cos \lambda_n y\,, \tag{29}$$

and after some algebraic manipulations

$$\theta = \frac{1+a}{as^2}\left(\hat{u} + \frac{2}{MU}\sum_{n=1}^{\infty} \frac{(-1)^n}{\lambda_n^3}\left(1 - \frac{\cosh \lambda_n z}{\cosh \lambda_n a}\right)\cos \lambda_n y\right) \tag{30}$$

The bulk mean temperature should be calculated as

$$\theta_m = \frac{1+a}{a^2 s^2}\int_0^1\int_0^a \left(\hat{u}^2 + \frac{2\hat{u}}{MU}\sum_{n=1}^{\infty} \frac{(-1)^n}{\lambda_n^3}\left(1 - \frac{\cosh \lambda_n z}{\cosh \lambda_n a}\right)\cos \lambda_n y\right) dz dy \tag{31}$$

The above equation along with Eq. (3-b) gives the Nusselt number.

3. Results and discussions

It should be noted that throughout this section we assumed $F=F_t=M=1$ and $\gamma=1.4$ though the closed form solutions are general enough to account for other values of the above parameters. As a sample of the results, Fig. 2 compares our *fRe* and β with those of (Morini et al. 2004) and (Tunc and Bayazitoglu 2002) for microducts without a porous insert, i.e. when $s=0$ and $a=1$. Seemingly, the results are in complete agreement.

Fig. 3 illustrates β, *fRe*, and *Nu* versus *s* for different aspect ratios with $Kn=0.001$. As seen, either of the above variables increases with both *s* and *a*. Higher values of *s* (with a fixed microduct size) can be interpreted as a decrease in the permeability of the porous medium. Therefore, the increase in *fRe* (which is linearly proportional to the pressure drop) is expected. It should be noted that *fRe* increases from O(10) to O(10^6) when *s* changes from unity to 10^3. Note that *fRe* is different from $C_f Re$ defined by Hooman and Merrikh (Hooman and Merrikh 2006) in such a way that the former is based on the total pressure drop but the latter is a measure of wall shear stress.

At the same time, with lower permeability the velocity distribution tends to be more uniform leading to an increase in *Nu* as noted for porous macroducts, see for example Hooman and Ranjbar-Kani (Hooman and Ranjbar-Kani 2003). Generally speaking, for this value of *Kn*, the plots of *Nu* are very similar to those of Haji-Sheikh (Haji-Sheikh 2006) and Hooman and Merrikh (Hooman and Merrikh 2006). The increase in β can be attributed to the fact that increasing *s*, as noted above, the velocity puts on uniform values in the regions far away from the walls while velocity changes will be restricted to a thin near-wall region. This means that velocity gradients are more severe near the walls leading to higher slip velocity. It is expected that with further increase in *s* all of the graphs, for different cross-sections, merge to an asymptotic maximum value for β.

Figs. 4 and 5 are designed to show the effects of *Kn* on β, *fRe*, and *Nu* for different aspect ratios (*a* values) with *s=4* and *s=1000,* respectively. It can be verified that for both of the *s* values *fRe* and *Nu* decrease with *Kn* similar to what reported for non-porous microducts. On the other hand, higher *Kn* can lead to higher slip velocity and hence β increases with *Kn* regardless of *s*. It is worth noting that, for s=1000 the plots of β merge asymptotically to β=1 as *Kn* increases while with lower *Kn* values the curves for a>4 are almost indistinguishable. It is worth commenting that the change in *Nu* is more severe for higher *a* values. For example, considering the case when s=4, with a change in *Kn* from 0.001 to 0.1, *Nu* changes nearly 50% when $a\rightarrow\infty$ (highlighted as PPC in this work) while this number figures out at 25% with a=1. According to Fig.5, with s=1000, *Nu* plunges about 75% and 50% with PPC and a=1, respectively. This fact drives home the point that alteration in *Nu*, with a change in *Kn*, is more pronounced at higher *s* values. Another interesting observation is that, with s=1000, *fRe* remains almost independent of *Kn*. The reason is that for very high values of *s*, say s>100, *fRe* is almost independent of the boundary friction (Brinkman) term as the Darcy viscous drag is predominant, see Kaviany . One can come up with this conclusion by a simple scale analysis of the momentum equation to observe that not only

fRe=O(s^2) for very high values of s but also fRe is independent of rarefaction effects that can kick in via the Brinkman shear stress term.

In Figs. 3-5 the Prandtl number value was fixed at 0.7 so there is a need to see its effect on the Nusselt number. Fig. 6 demonstrates the Nusselt number versus Kn for different Pr and a values with s=10. Observe that, for each aspect ratio, Nu increases with Pr and this effect becomes more pronounced as Kn increases. It is not surprising as one knows that Nu is independent of Pr for no-slip laminar flow.

4. A case study

As an example we consider the microporous heat sink concept proposed by Lage and co-workers (Lage et al. 1996, Antohe et al. 1996, Nield, Porneala and Lage 1999) in cooling phased-array radar that remains fixed and is electronically steered to look in all directions where a typical cold-plate for a phased-array radar system consisting of an enclosure measuring 500x150x1mm in width, depth, and height, respectively (Lage et al. 1996). A very similar design based on flow of air, with λ=4μ, through an identical Al-foam is assumed here with ε=0.4, s=1000, and q''=7kW/m^2. Before proceeding to calculate the inlet-outlet temperature difference that can be achieved by this system, it is instructive to remind the reader of convection heat transfer coefficient, h, which is defined as

$$h= q''/(T_w^*-T_m^*). \quad (32)$$

Combining it with the Nusselt number definition, Eq. (19), one has $h=kNu/D_H$. This conclusion is very important to describe the performance of the microporous duct. As seen, decreasing the duct dimension the heat transfer coefficient increases. However, it should be noted that decreasing the duct size will, at the same time, increase Kn that, in turn, will reduce Nu and hence h, see for example (Hooman 2007). It seems that there is a trade-off between these two, say, favorable and adverse effects of downsizing the microduct. For instance, moving from D_H=2mm to 0.2mm,

while h is inverse-linearly proportional to D_H, with s=1000, the Nusselt number reduces about 13%.

Another point in favor of a microporous duct is that, as an effective thermal conductivity k is much higher than (several order of magnitude) that of fluid, air, in this case. A rough and ready estimate for the effective thermal conductivity is the linear superposition of that of fluid and the matrix as $k= \varepsilon k_f+(1- \varepsilon)k_{pm}$. Details on other alternative formulae for the effective thermal conductivity can be found in (Nield and Bejan 2006) and are not repeated here. Similar to (Lage et al. 1996), one sets k_{pm}=170W/mK and k_f=0.025W/mK that leads to k=102W/mK. Consequently, for D_H=2mm the heat transfer coefficient can be as high as h=51Nu (Kw/m^2) where the no-slip Nu, that maximizes h, is Nu=12. This leads to h_{max}=612 (Kw/m^2) which is a remarkable value especially when one observes that the fully developed value of h is always less than its developing counterpart, see for example (Mousavi and Hooman 2006, Hooman and Gurgenci 2007b, Haddad, Ali-Nimr and Sari 2007).

Another issue of interest is to find the mean inlet-outlet temperature difference for the above-described system. This can be achieved by introducing a thermal resistance defined as $R=(T^*_{m,o}-T^*_{m,in})/q''$, see Kaviany (Kaviany 2002) for more details on the thermal resistance concept. Application of the First Law of Thermodynamics to the whole microporous duct leads to

$$R=\frac{T^*_{m,o}-T^*_{m,in}}{q''}=\frac{1}{\rho c_P U^*}\frac{4L}{D_H} \qquad (33)$$

This is a general conclusion regardless of the permeability, rarefaction, and the fully developed assumption.

Figure 7 presents the thermal resistance versus the fluid inlet velocity for 3 different microduct sizes. Note that R is inverse-linearly proportional to U^* and D_H. Hence, with a fixed L, one has a quantitative clue on how reducing the duct size can affect the heat transfer performance of the system. Moreover, according to Eq. (33), with a fixed U^* plots of R versus D_H should be identical

to those of R versus U^*. As seen, with a fixed heat flux, the highest temperature difference can be achieved for the smallest size for which slip effects are not negligible as one has Kn=0.02.

Keep in mind that in this case D_H=*0.2/20 mm* with a fixed permeability leads to $s=10^2/10^4$ while we assumed s remains unchanged when the duct size alters, i.e. s=1000. Nonetheless, one can consult (Hooman and Merrikh 2006) to observe that Nu is almost independent of s when s>O(10). This means that even with s=100 results of this case study are acceptable. The reader; however, is warned that doing another case study for smaller s values, one should carefully monitor the changes in the system performance due to the so-called favorable and adverse effects of downsizing when it comes to find h.

5. Conclusion

Applying the Brinkman flow model, closed form solutions for fully developed velocity and temperature distribution in a porous microchannel of rectangular cross-section is presented with the effects of velocity slip and temperature jump being considered. The **H1** thermal boundary condition is assumed to be valid for the micro-porous duct. Convection heat transfer and pressure drop performance of the system, reflected in Nu and fRe, respectively, were analyzed. Effect of the Knudsen and the Prandtl number, the porous media shape parameter, the inlet velocity, the duct size, and the duct geometry on the system performance is studied. The proposed results are general enough to be applied to a microporous rectangular duct. Furthermore, as with s=0 the Brinkman flow model reduces to the fully developed Navier-Stokes equations, the present results are applicable to clear fluid case.

Acknowledgments

Financial support provided by The University of Queensland in terms of UQILAS, Endeavor IPRS, and School Scholarship is appreciated. The author is also indebted to anonymous reviewers for their improving suggestions.

References

Ameel, T. A., X. M. Wang, R. F. Barron & R. O. Warrington (1997) Laminar forced convection in a circular tube with constant heat flux and slip flow. *Microscale Thermophysical Engineering,* 1**,** 303-320.

Antohe, B. V., J. L. Lage, D. C. Price & R. M. Weber (1996) Numerical characterization of micro heat exchangers using experimentally tested porous aluminum layers. *International Journal of Heat and Fluid Flow,* 17**,** 594-603.

Beck, J. v., K. Cole, A. Haji-Sheikh & B. Litkouhi. 1992. *Heat Conduction Using Green's Functions,* . Washington D. C.: Hemisphere Publ. Corp., .

Ghodoossi, L. & N. Egrican (2005) Prediction of heat transfer characteristics in rectangular microchannels for slip flow regime and H1 boundary condition. *International Journal of Thermal Sciences,* 44**,** 513-520.

Haddad, O. M., M. A. Al-Nimr & M. M. Abuzaid (2006) Effect of periodically oscillating driving force on basic microflows in porous media. *Journal of Porous Media,* 9**,** 695-707.

Haddad, O. M., M. A. Al-Nimr & J. S. Al-Omary (2007) Forced convection of gaseous slip-flow in porous micro-channels under Local Thermal Non-Equilibrium conditions. *Transport in Porous Media,* 67**,** 453-471.

Haddad, O. M., M. A. Ali-Nimr & M. S. Sari (2007) Forced convection gaseous slip flow in circular porous micro-channels. *Transport in Porous Media,* DOI 10.1007/s11242-006-9093-0.

Haddad, O. M., M. A. Ali-Nimr & Y. Taamneh (2006) Hydrodynamic and thermal behavior of gas flow in microchannels filled with porous media. *Journal of Porous Media,* 9**,** 403-414.

Haji-Sheikh, A. (2006) Fully developed heat transfer to fluid flow in rectangular passages filled with porous materials. *Journal of Heat Transfer-Transactions of the Asme,* 128**,** 550-556.

Haji-Sheikh, A., W. J. Minkowycz & E. M. Sparrow (2004) Green's function solution of temperature field for flow in porous passages. *International Journal of Heat and Mass Transfer,* 47**,** 4685-4695.

Haji-Sheikh, A., D. A. Nield & K. Hooman (2006) Heat transfer in the thermal entrance region for flow through rectangular porous passages. *International Journal of Heat and Mass Transfer,* 49**,** 3004-3015.

Haji-Sheikh, A. & K. Vafai (2004) Analysis of flow and heat transfer in porous media imbedded inside various-shaped ducts. *International Journal of Heat and Mass Transfer,* 47**,** 1889-1905.

Hooman, K. (2007) Entropy generation for microscale forced convection: Effects of different thermal boundary conditions, velocity slip, temperature jump, viscous dissipation, and duct geometry. *International Communications in Heat and Mass Transfer,* 34**,** 945-957.

Hooman, K. & H. Gurgenci (2007a) Effects of temperature-dependent viscosity variation on entropy generation, heat and fluid flow through a porous-saturated duct of rectangular cross-section. *Applied Mathematics and Mechanics-English Edition,* 28**,** 69-78.

--- (2007b) Effects of viscous dissipation and boundary conditions on forced convection in a channel occupied by a saturated porous medium. *Transport in Porous Media,* 68**,** 301-319.

Hooman, K., H. Gurgenci & A. A. Merrikh (2007) Heat transfer and entropy generation optimization of forced convection in a porous-saturated duct of rectangular cross-section. *International Journal of Heat and Mass Transfer,* 50**,** 2051-2059.

Hooman, K., A. Haji-Sheikh & D. A. Nield (2007) Thermally developing Brinkman-Brinkman forced convection in rectangular ducts with isothermal walls. *International journal of Heat and Mass Transfer,* 50**,** 3521-3533.

Hooman, K. & A. A. Merrikh (2006) Analytical solution of forced convection in a duct of rectangular cross section saturated by a porous medium. *Journal of Heat Transfer-Transactions of the Asme,* 128**,** 596-600.

Hooman, K. & A. A. Ranjbar-Kani (2003) Forced convection in a fluid-saturated porous-medium tube with isoflux wall. *International Communications in Heat and Mass Transfer,* 30**,** 1015-1026.

Kaviany, M. 2002. *Principles of heat transfer* New York Wiley.

Kreyszig, E. 2006. *Advanced engineering mathematics* Hoboken, NJ John Wiley.

Lage, J. L., A. K. Weinert, D. C. Price & R. M. Weber (1996) Numerical study of a low permeability microporous heat sink for cooling phased-array radar systems. *International Journal of Heat and Mass Transfer,* 39**,** 3633-3647.

Merrikh, A. A. & J. L. Lage (2005) The role of red cell movement on alveolar gas diffusion. *Materialwissenschaft Und Werkstofftechnik,* 36**,** 497-504.

Morini, G. L., M. Spiga & P. Tartarini (2004) The rarefaction effect on the friction factor of gas flow in microchannels. *Superlattices and Microstructures,* 35**,** 587-599.

Mousavi, S. S. & K. Hooman (2006) Heat and fluid flow in entrance region of a channel with staggered baffles. *Energy Conversion and Management,* 47**,** 2011-2019.

Nield, D. A. & A. Bejan. 2006. *Convection in porous media* New York: Springer.

Nield, D. A. & A. V. Kuznetsov (2006) Forced convection with slip-flow in a channel or duct occupied by a hyper-porous medium saturated by a rarefied gas. *Transport in Porous Media,* 64**,** 161-170.

Nield, D. A., D. C. Porneala & J. L. Lage (1999) A theoretical study, with experimental verification, of the temperature-dependent viscosity effect on the forced convection through a porous medium channel. *Journal of Heat Transfer-Transactions of the Asme,* 121**,** 500-503.

Renksizbulut, M., H. Niazmand & G. Tercan (2006) Slip-flow and heat transfer in rectangular microchannels with constant wall temperature. *International Journal of Thermal Sciences,* 45**,** 870-881.

Sparrow, E. M. & A. Hajisheikh (1964) Velocity Profile and Other Local Quantities in Free-Molecule Tube Flow. *Physics of Fluids,* 7**,** 1256-1261.

Tunc, G. & Y. Bayazitoglu (2002) Heat transfer in rectangular microchannels. *International Journal of Heat and Mass Transfer,* 45**,** 765-773.

Yu, S. P. & T. A. Ameel (2001) Slip-flow heat transfer in rectangular microchannels. *International Journal of Heat and Mass Transfer,* 44**,** 4225-4234.

Zhu, X. & Q. Liao (2006) Heat transfer for laminar slip flow in a microchannel of arbitrary cross section with complex thermal boundary conditions. *Applied Thermal Engineering,* 26**,** 1246-1256.

Zhu, X., Q. Liao & M. D. Xin (2006) Gas flow in microchannel of arbitrary shape in slip flow regime. *Nanoscale and Microscale Thermophysical Engineering,* 10**,** 41-54.

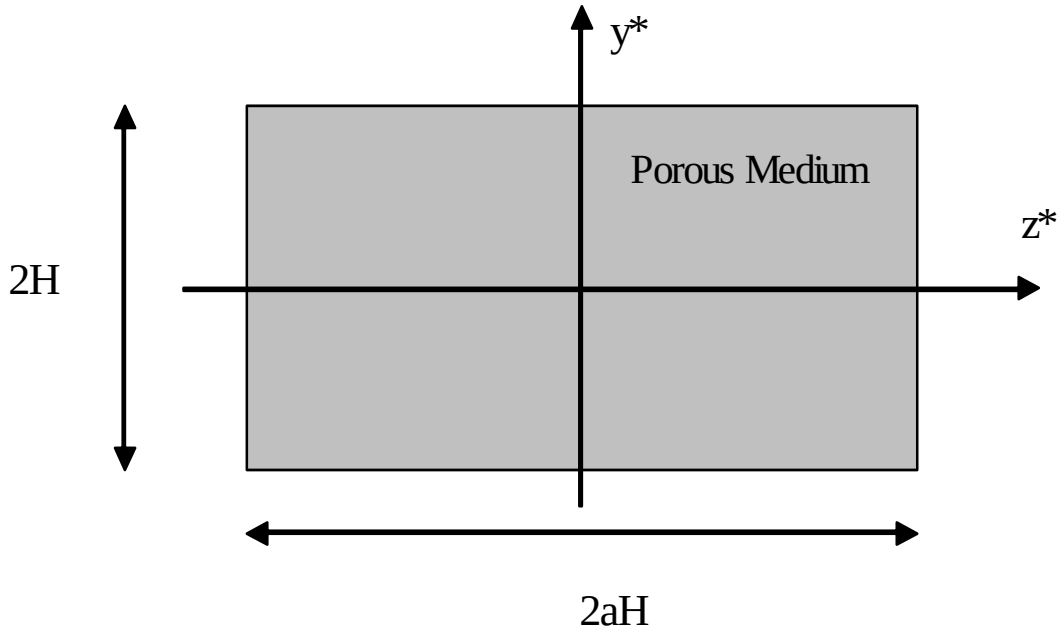

Fig. 1 Definition sketch.

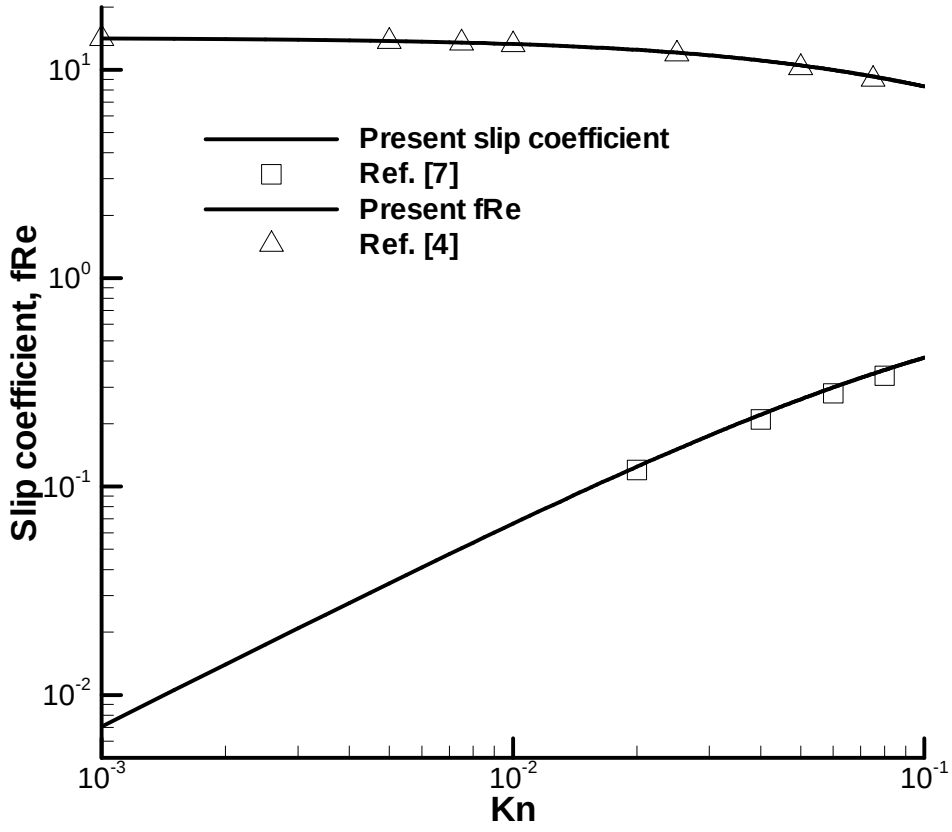

Fig.2 β and fRe versus Kn compared with previous results in the literature for s=0.

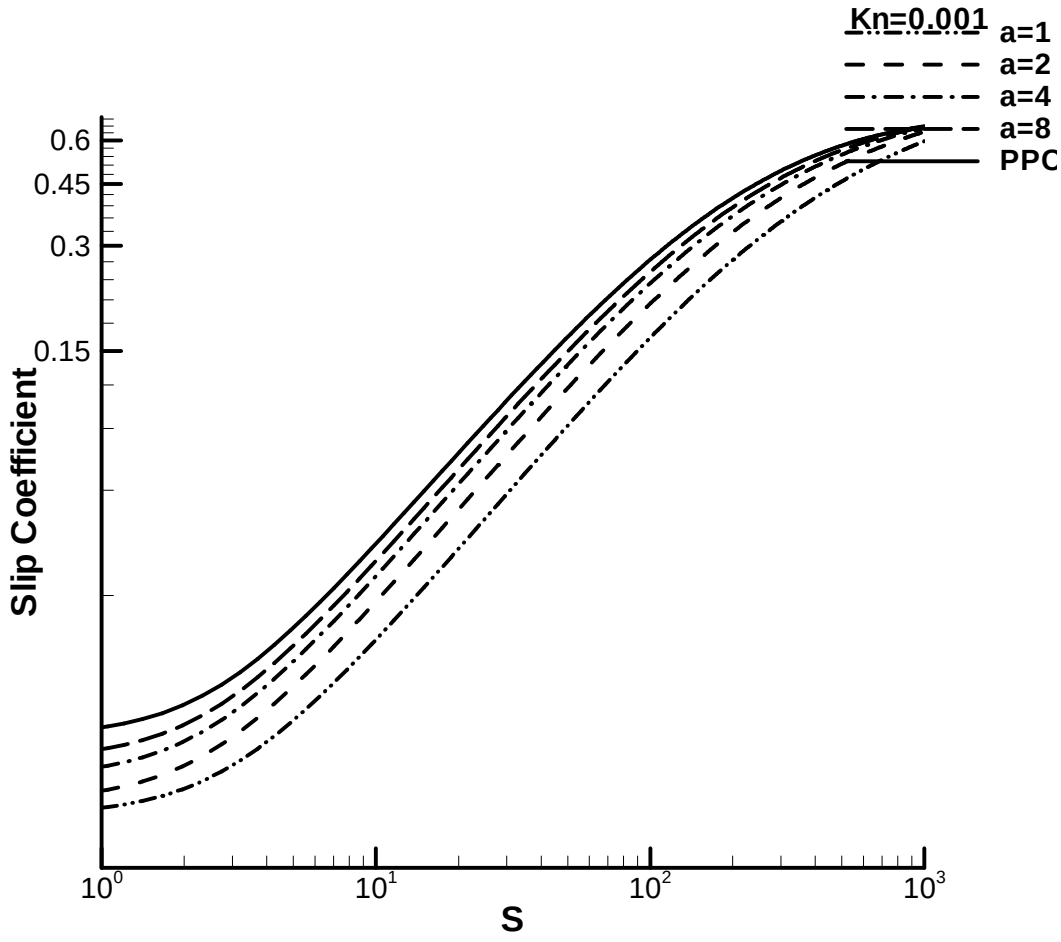
Kn=0.001
a=1
a=2
a=4
a=8
PPC
0.6
0.45
0.3
0.15
Slip Coefficient
10^0
10^1
10^2
10^3
S

(a)

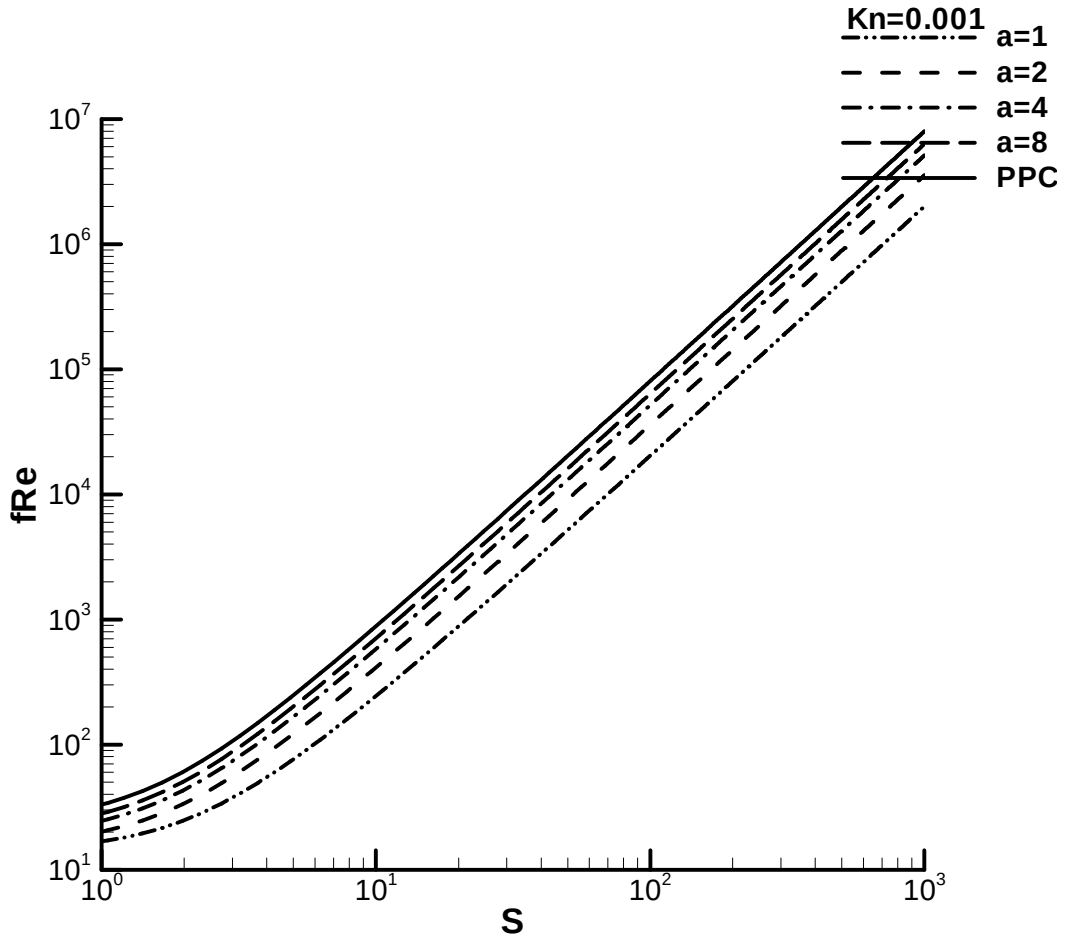
Kn=0.001
a=1
a=2
a=4
a=8
PPC
fRe
S
10^7
10^6
10^5
10^4
10^3
10^2
10^1
10^0
10^1
10^2
10^3

(b)

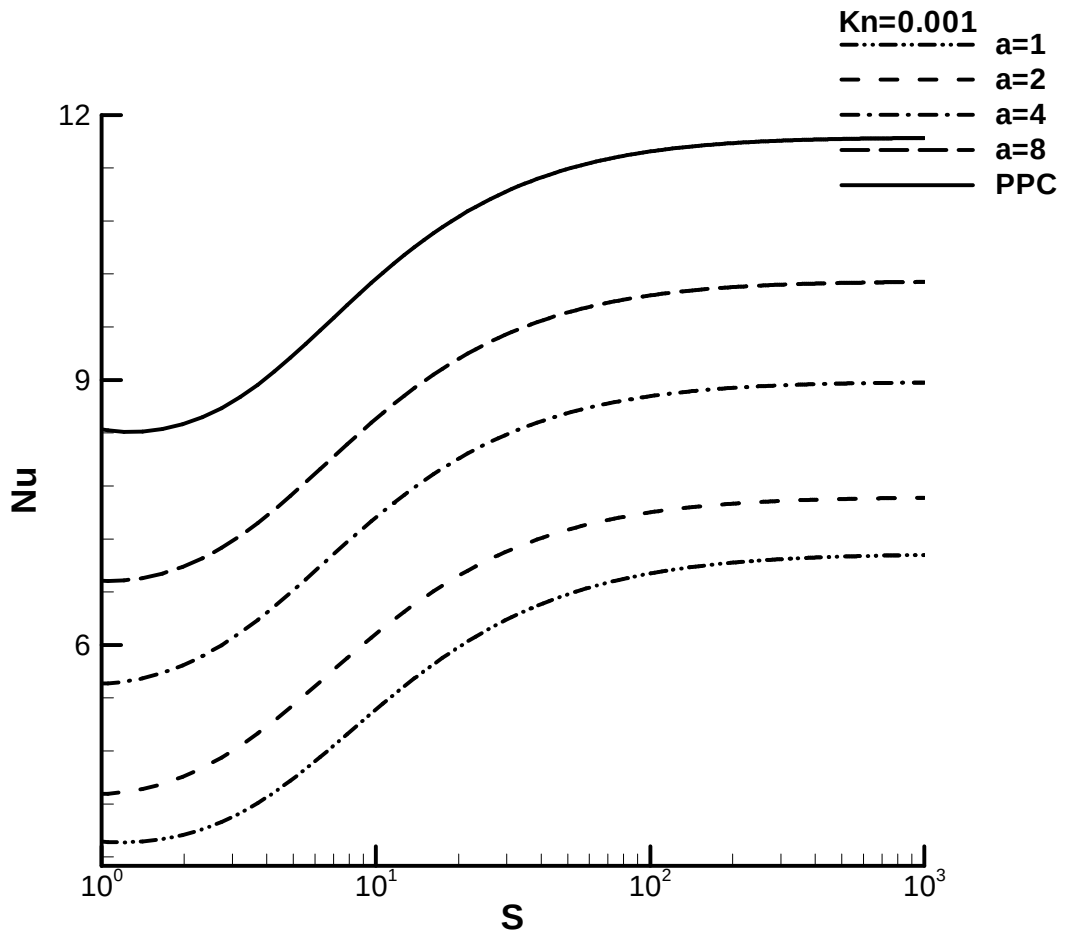

(c)

Fig. 3 a) Slip coefficient b)fRe c)Nu versus s for Kn=0.001

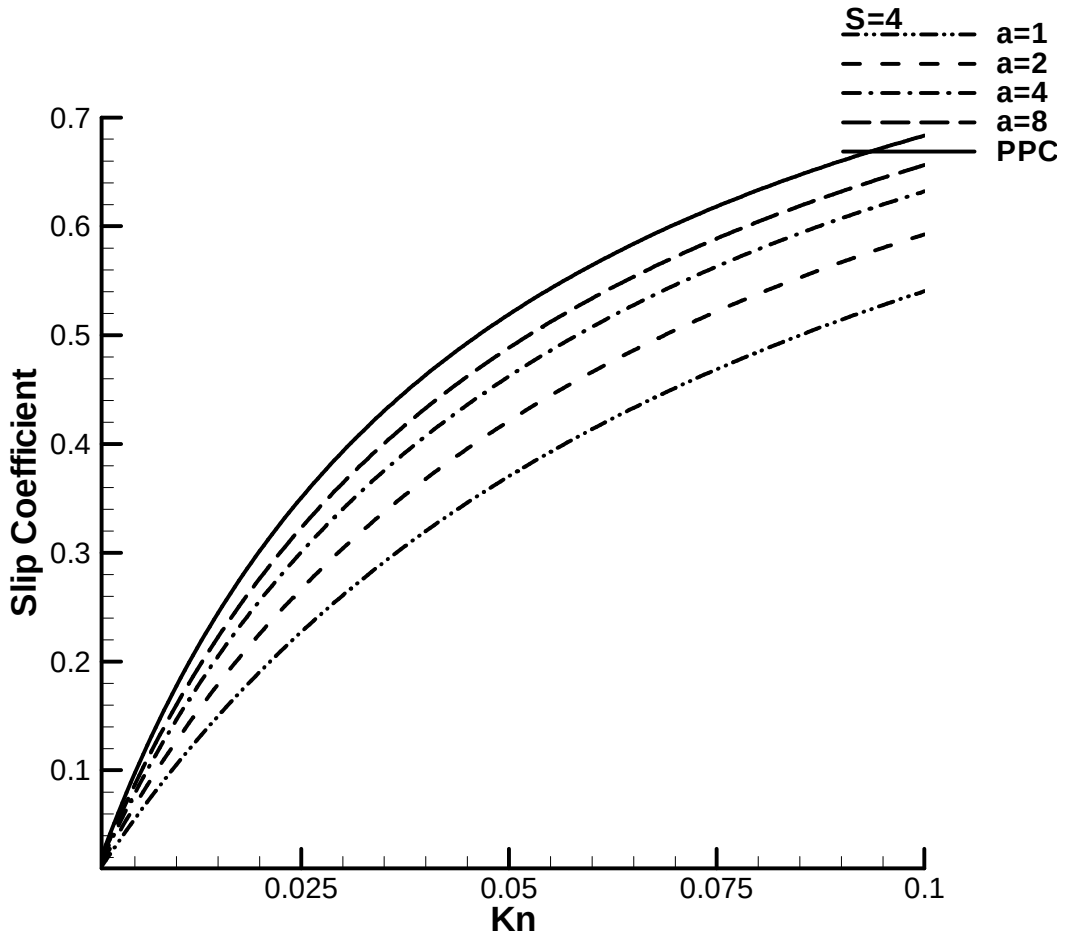
S=4
a=1
a=2
a=4
a=8
PPC
Slip Coefficient
0.7
0.6
0.5
0.4
0.3
0.2
0.1
0.025
0.05
0.075
0.1
Kn

(a)

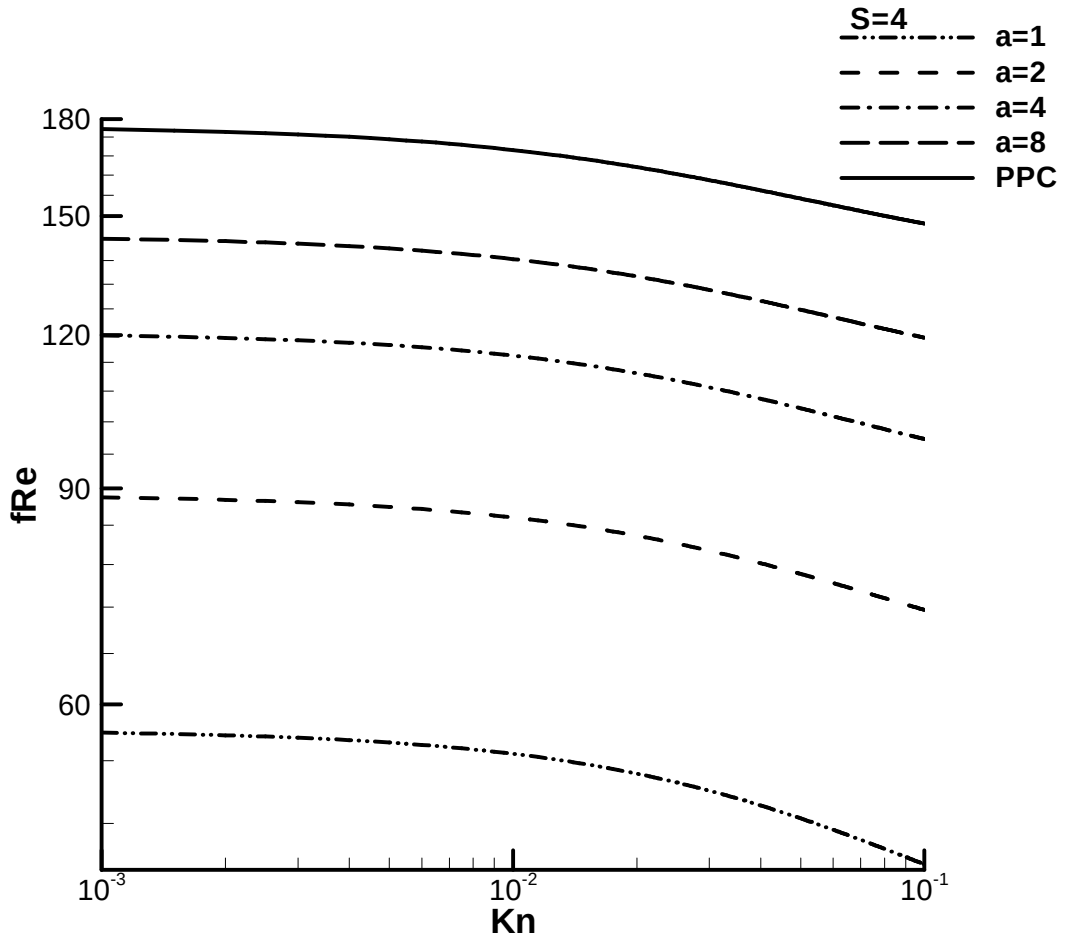

(b)

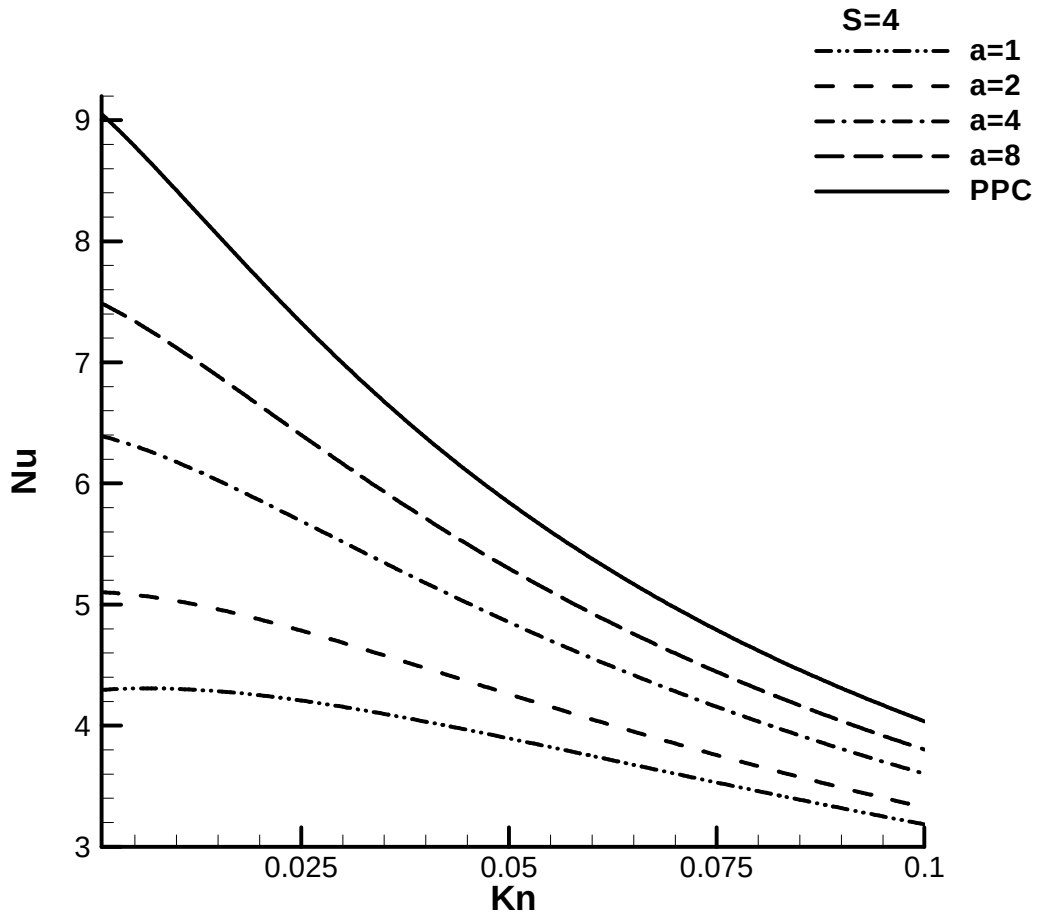

(c)

Fig. 4 a) Slip coefficient b)fRe c)Nu versus Kn with S=4 for different aspect ratios

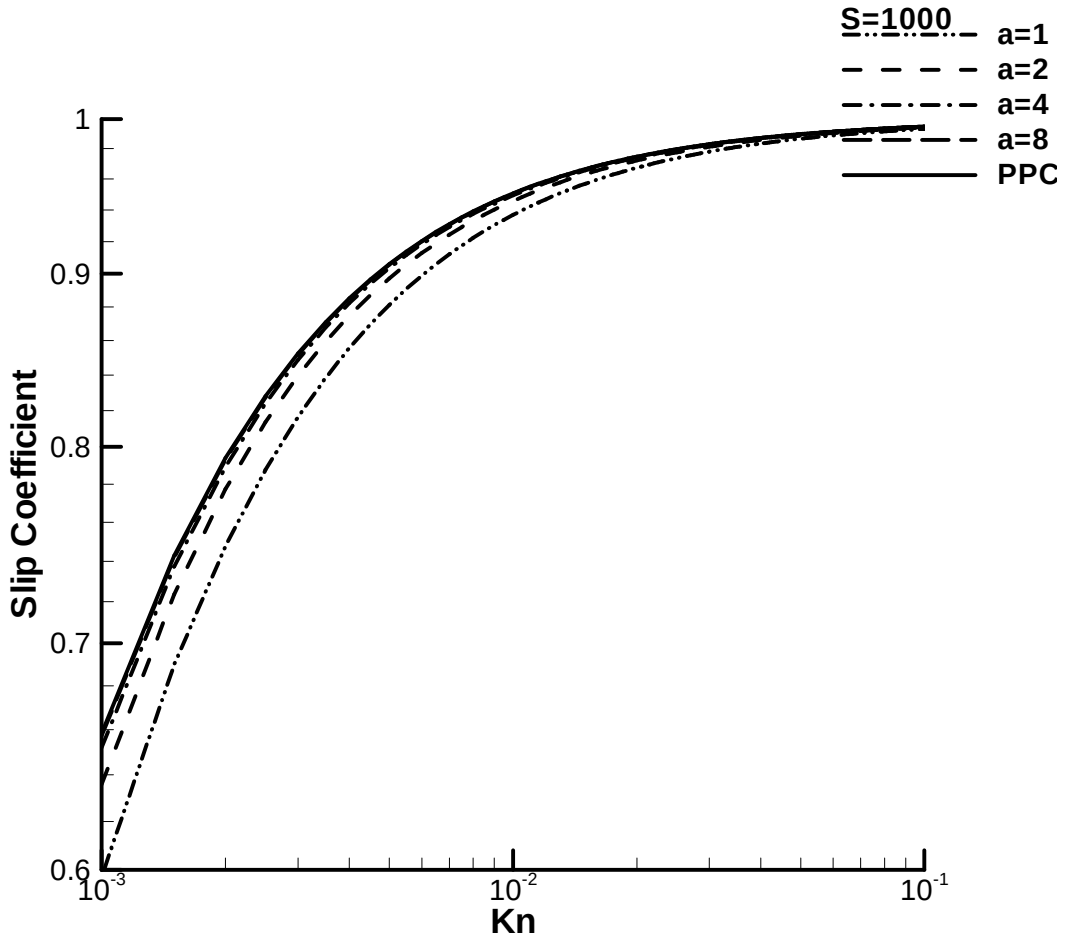
S=1000
a=1
a=2
a=4
a=8
PPC
Slip Coefficient
1
0.9
0.8
0.7
0.6
10-3
10-2
10-1
Kn

(a)

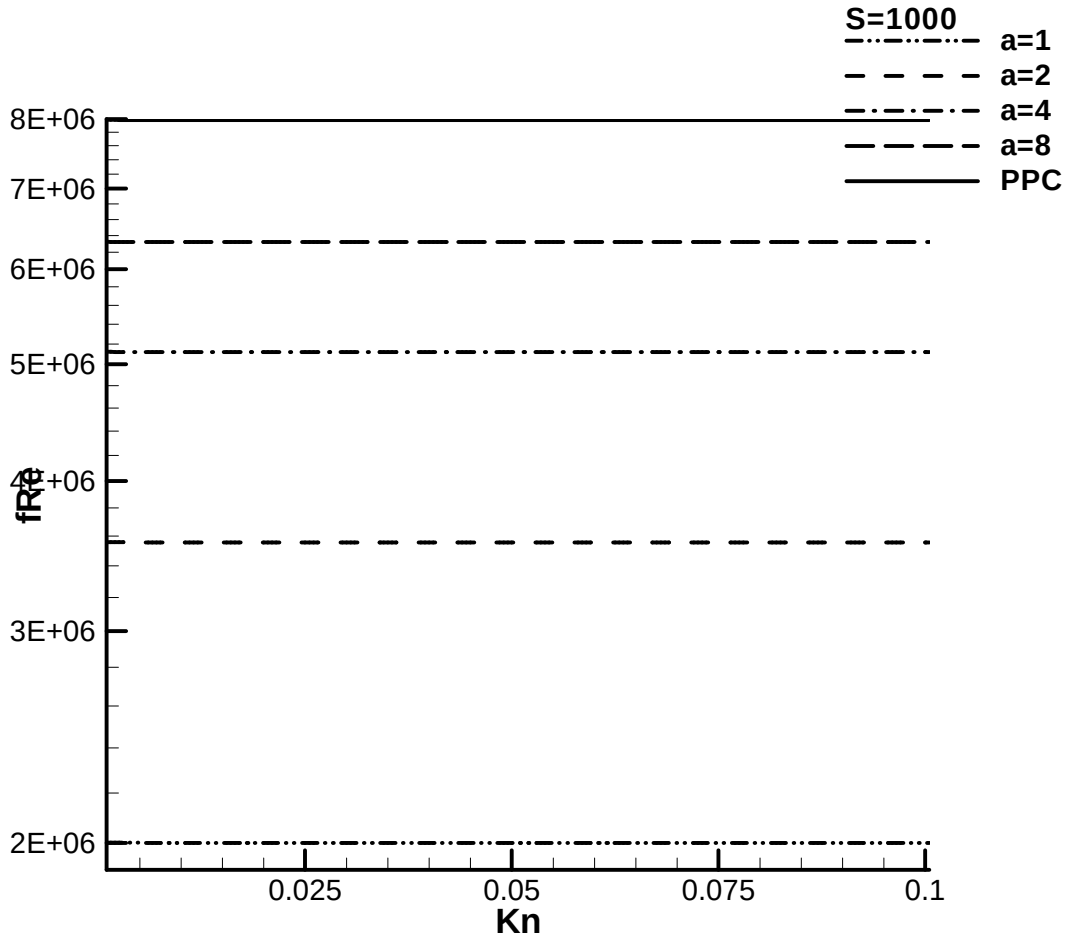
S=1000
a=1
a=2
a=4
a=8
PPC
8E+06
7E+06
6E+06
5E+06
4E+06
3E+06
2E+06
fRe
0.025
0.05
0.075
0.1
Kn

(b)

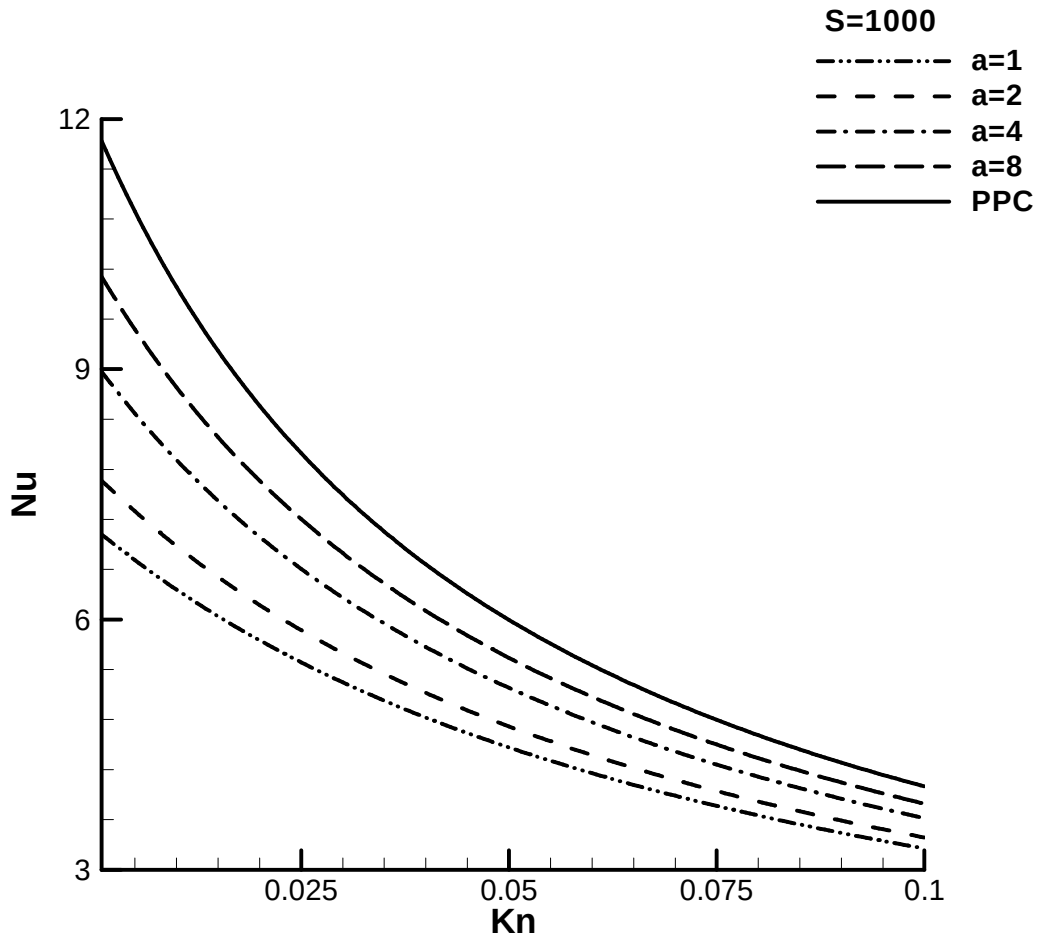

(c)

Fig. 5 a) Slip coefficient b)fRe c)Nu versus Kn with $S=10^3$ for different aspect ratios

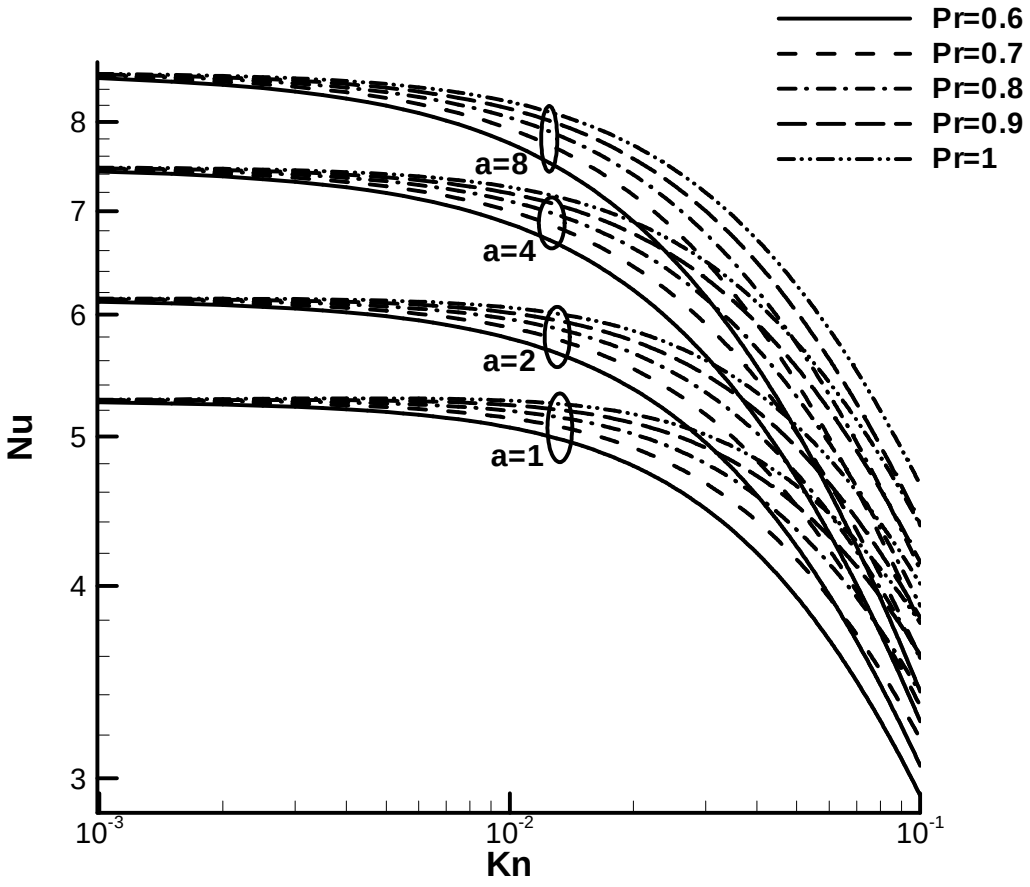

Fig. 6 The Nusselt number versus Kn for different Pr and a values with S=10.

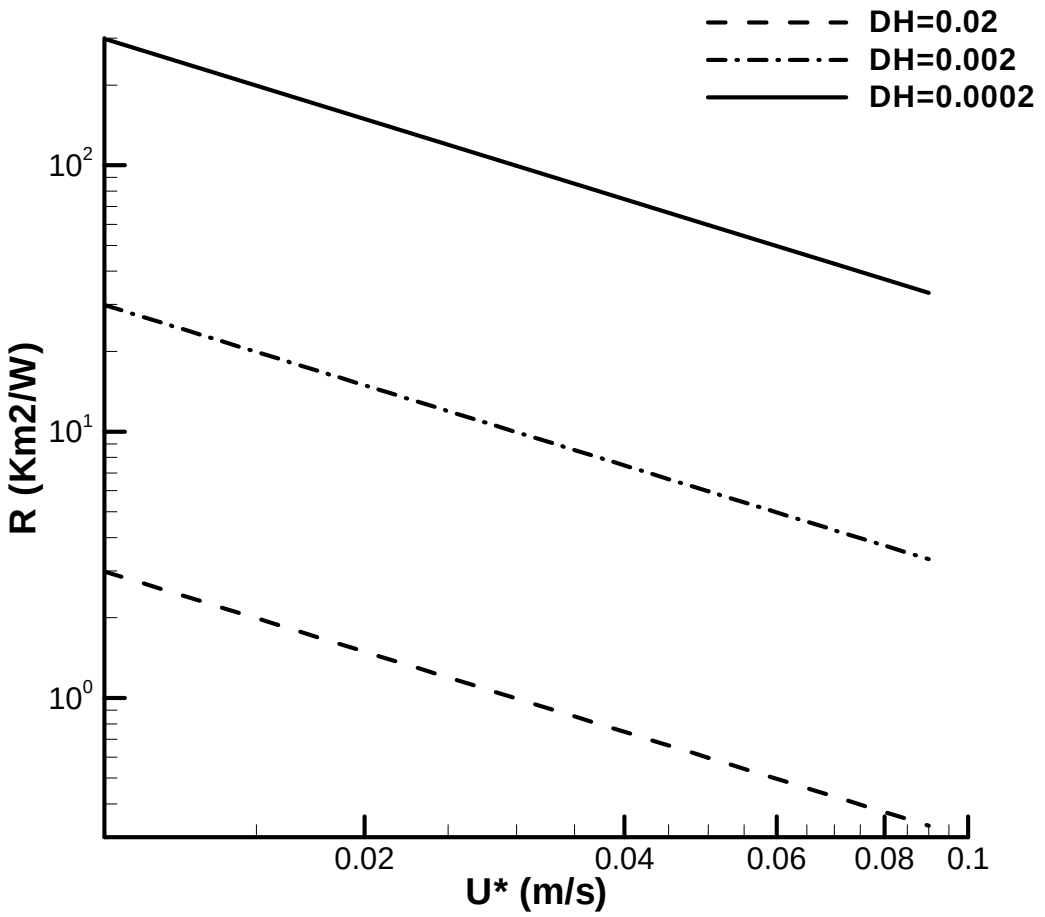

Fig. 7 Thermal resistance versus inlet velocity for different duct sizes, S=1000.